Modeling the Substituent Effect on the Oxidative Degradation of Azo Dyes

Alimet Sema Özen and Viktorya Aviyente*

Department of Chemistry, Bogazici University, 34342 Bebek-Istanbul, Turkey

Frank De Proft and Paul Geerlings

Eenheid Algemene Chemie, Faculteit Wetenschappen, Vrije Universiteit Brussel (VUB), Pleinlaan 2, 1050 Brussels, Belgium

Received: October 16, 2003; In Final Form: April 27, 2004

In this paper, using DFT methods and reactivity indices, we show that the oxidative degradation of azo dyes occurs through the cleavage of the N−N bond following the hydroxyl radical addition to the chromophore. The geometries for two experimentally proposed reaction pathways regarding the cleavage of the C−N and N−N bonds for Cl- and CH_3-substituted azo dye 4-(4′-sulfophenylazo)phenol are optimized at the B3LYP/6-31G(d) level of theory, and energies are further refined by single-point calculations at MPW1K/6-31+G(d,p)//B3LYP/6-31G(d). Potential energy surfaces (PES) are compared for the two mechanisms to determine the energetically more favorable mechanism as well as to explain the huge reactivity difference between the Cl- and CH_3-substituted derivatives. Reactivity indices are used in the search for competing reactions.

Introduction

The degradation of azo dyes, which are found in the wastewater of the textile industry, has been of great environmental concern because azo dyes do not respond well to conventional treatment methods. The use of advanced oxidation processes (AOPs), through oxidative cleavage reactions with hydroxyl radicals, however, appears to be a promising new technique for the degradation of such unmanageable waste. Using high-performance liquid chromatography (HPLC) and mass spectrometry (MS), two mechanisms involving either C−N or N−N bond cleavages have been proposed for the oxidative cleavage reaction of azo dyes.

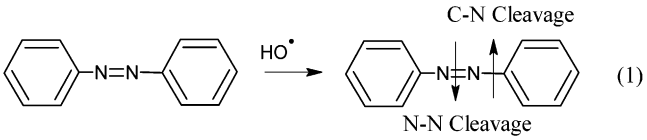

(1)

According to these mechanisms, a hydroxyl radical attacks either the carbon atom bearing the azo linkage, leading to the cleavage of the C−N bond and the generation of benzene,[1−10] or the nitrogen atom, followed by the cleavage of the N−N bond resulting in the formation of nitrosobenzene.[11−15] Both of these experimentally proposed mechanisms have been studied by means of quantum mechanical calculations using density functional theory (DFT) methods, chemical reactivity indices, and electron density topology,[16] and it was found that the N−N bond cleavage mechanism was preferable over the C−N bond cleavage mechanism. The rapid disappearance of color in dye solutions, as well as the fact that mineralization was found to be the rate-determining step, was justified by the N−N cleavage mechanism. As a matter of fact, it was concluded that the presence of the hydrazone tautomer in experimental studies, rather than the azo tautomer, could be indicative of the mechanism involving C−N bond cleavage.

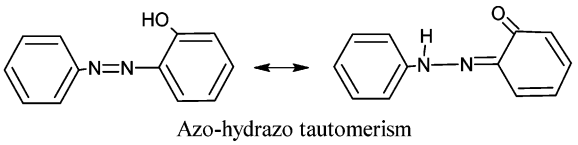

(2)

Azo-hydrazo tautomerism

As the experimental studies show, the rate of azo dye oxidation is dependent on the dye structure[3,12,16] and the nature of the substituents.[3] In recent work, Nam et al. have reported the substituent effect on azo dye oxidation by the Fe^{III}−EDTA−H_2O_2 system for methyl-, methoxy-, and halogen-substituted dyes and model compounds. They have found that halogen-substituted dyes were decolorized to a greater extent and more rapidly.[3] The aim of this study is to examine the substituent effects on the oxidative degradation of azo dyes using a computational and conceptual DFT approach,[17−21] as well as to check the validity of the most plausible mechanism that was determined for the unsubstituted model compound, azo benzene.[16]

In this study, because of the large reactivity difference toward decolorization,[3] 2-methyl- and 2-chloro- derivatives of 4-(4′-sulfophenylazo)phenol have been chosen to determine the substituent effect on the oxidative degradation of azo dyes. Absorbance decreases at λ_{max} are 30 and 95% for CH_3 (**1_{Me}**) and Cl (**1_{Cl}**) substitution, respectively,[3] indicating a better degradation yield for the chloro-substituted derivative.

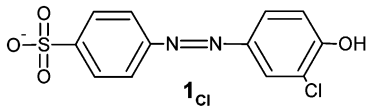

1_{Cl}

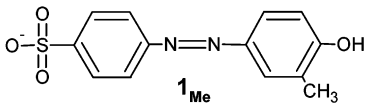

1_{Me}

* Corresponding author. E-mail. aviye@boun.edu.tr.

10.1021/jp037138z CCC: $27.50
Published on Web 06/17/2004

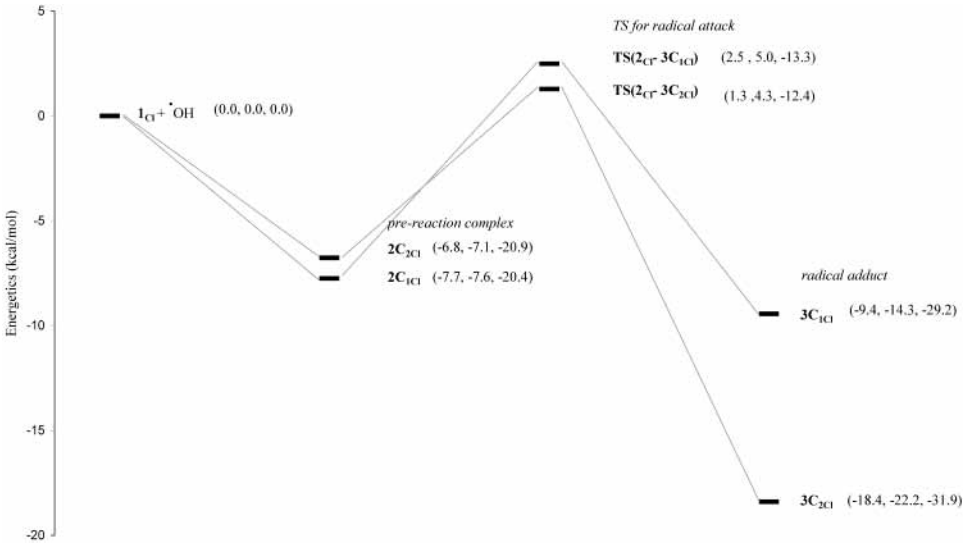

Figure 1. Potential energy profile for the hydroxyl radical addition mechanism in the C−N bond-cleavage pathway of the Cl-substituted azo dye at the B3LYP/6-31G(d) level. Relative energies in parentheses in the format of (B3LYP/6-31G(d), MPW1k/6-31+G(d,p)//B3LYP/6-31G(d), and IEFPCM) values. (0.0 kcal/mol on the relative-energy axis corresponds to $\mathbf{1_{Cl}}$ + •OH = (−1806.377834, −1806.138183, −1806.670002) hartrees with the same format.)

SCHEME 1: Mechanism for Radical Addition in C−N Bond Cleavage Pathway (X=Cl, Me)

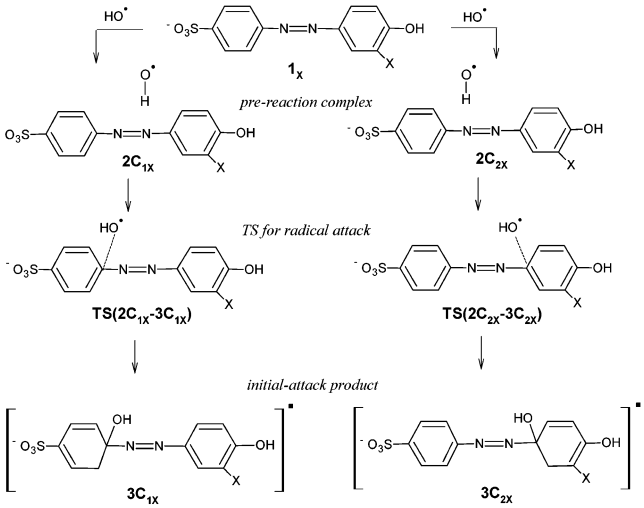

Theoretical Background

DFT and DFT-Based Reactivity Descriptors. Modeling the oxidative degradation of azo compounds involves radical reactions or open-shell molecules that are considered challenges in electronic structure methods because of the problem of spin contamination. However, DFT methods[17−19] are good candidates for calculations involving open-shell systems because they seem to suffer to a lesser extent from spin contamination.[22,23] They are also more efficient for large systems in terms of computer time compared to post-HF methods such as MP2.

Furthermore, DFT methods may be used not only to calculate molecular properties, potential energy surfaces, and the course of a given reaction but also are very useful tools for obtaining conceptual information about chemical reactivity as well as for treating qualitative concepts such as hardness and electronegativity.[17,20,21]

Because the electron density is considered to contain all the information about the molecular properties, chemical reactivity should be reflected in the molecular sensitivity to perturbations of different types.[20,21] If the electronic energy is considered to

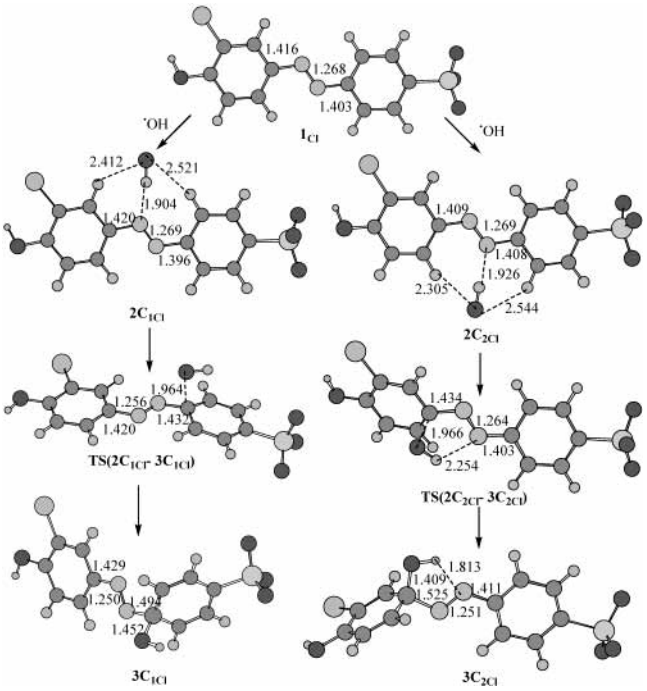

Figure 2. Optimized structures for hydroxyl radical addition in the C−N cleavage pathway of Cl-substituted azo dye, $\mathbf{1_{Cl}}$.

be a functional of the number of electrons and external potential, $E[N, v(\mathbf{r})]$, then these perturbations can be obtained by a series of derivatives of the energy. Perturbations due to changes in the number of electrons are defined as global properties and are related to overall molecular stability. Perturbations due to changes in external potential are called local properties and determine the site selectivity of a molecule for a specific reaction type.[20,21]

Chemical potential is a global property that measures the escaping tendency of an electronic cloud

$$\mu = \left(\frac{\delta E[N, v(\mathbf{r})]}{\delta N}\right)_{v(\mathbf{r})} \tag{3}$$

In the finite difference approximation, this is equivalent to the

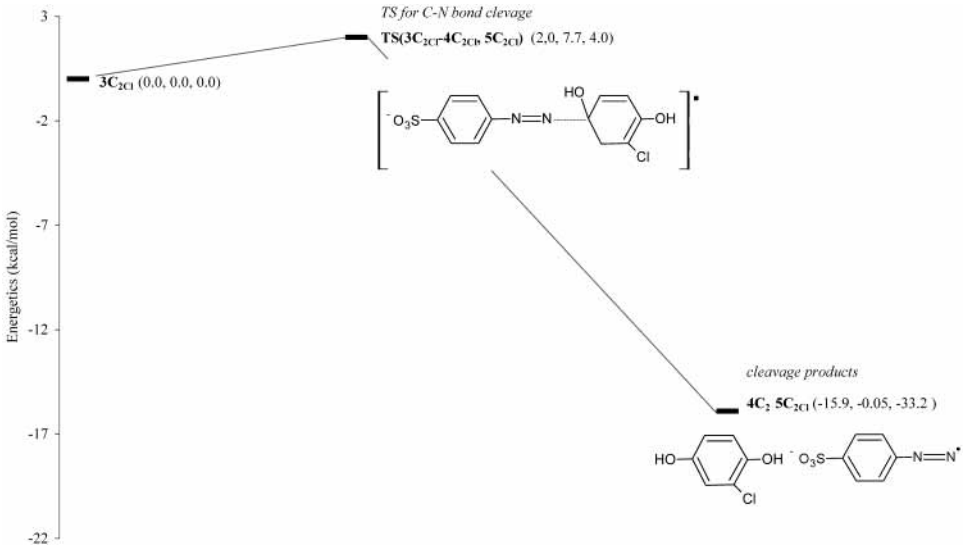

Figure 3. Potential energy profile for the representative C−N bond cleavage mechanism after the formation of the radical adduct for Cl-substituted azo dye at B3LYP/6-31G(d) level. Relative energies in parentheses in the format of (B3LYP/6-31G(d), MPW1k/6-31+G(d,p)//B3LYP/6-31G(d), and IEFPCM). (0.0 kcal/mol on the relative energy axis corresponds to $\mathbf{3C_{2Cl}}$ = (−1806.407145, −1806.3710077, −1806.692005) hartrees.)

negative of the average of the vertical ionization potential and electron affinity

$$\mu = \frac{-(I + A)}{2} \tag{4}$$

Electronegativity, χ, is defined as the negative of chemical potential

$$\chi = -\mu \tag{5}$$

Hardness is a global property described as the resistance to change in the electron distribution[24] that determines the stability of a molecule

$$\eta = \frac{\delta\mu}{\delta N} = \left(\frac{\delta^2 E[N, \mathrm{v}(\mathbf{r})]}{\delta N^2}\right)_{v(\mathbf{r})} \tag{6}$$

In the finite difference approximation, this is equivalent to

$$\eta \approx \frac{(I - A)}{2} \tag{7}$$

and for closed-shell molecules, it can be further approximated as the HOMO−LUMO energy gap. According to the maximum hardness principle, molecules arrange themselves to be as hard as possible.[24,25] Global softness S is the inverse of global hardness

$$S = \frac{1}{\eta} \tag{8}$$

Local softness $s(r)$ describes local perturbations in terms of electron density with respect to a global change in chemical potential

$$s(r) = \frac{\delta\rho(r)}{\delta\mu} \tag{9}$$

The Fukui function $f(r)$ is a space-dependent local function, and "it measures how sensitive a system's chemical potential is to an external perturbation at a particular point".[17] It also gives information about a quantity related to the electron density of an atom or molecule in its frontier regions.[17,26]

$$f(r) = \left(\frac{\delta\mu}{\delta v(\mathbf{r})}\right)_N = \left(\frac{\delta\rho(r)}{\delta N}\right)_{v(\mathbf{r})} \tag{10}$$

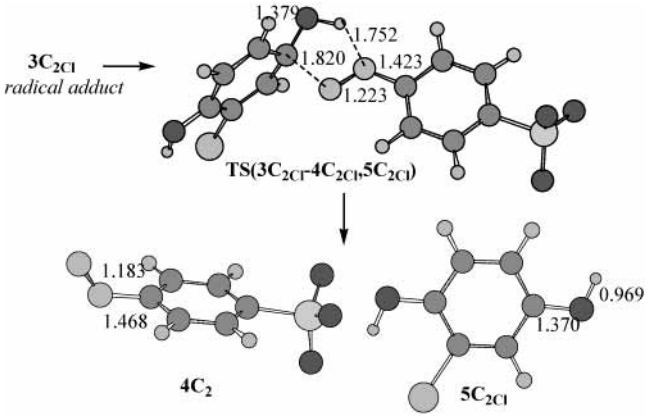

Figure 4. Optimized structures for the C−N cleavage pathway after the formation of the radical adduct for the Cl-substituted azo dye $\mathbf{1_{Cl}}$.

These two local properties are related to each other through global softness, S.

$$s(r) = f(r)\, S \tag{11}$$

However, because ${}^{\delta\rho(r)}/_{\delta N}$ is a discontinuous function of N, it will have one value from the right, one from the left, and an average at some integral value of N.

$$f^{+}(r) = \left[\frac{\delta\rho(r)}{\delta N}\right]^{+}_{v(\mathbf{r})} \quad (\text{as } N \text{ goes from } N_0 \text{ to } N_0 + \delta) \tag{12a}$$

$$f^{-}(r) = \left[\frac{\delta\rho(r)}{\delta N}\right]^{-}_{v(\mathbf{r})} \quad (\text{as } N \text{ goes from } N_0 - \delta \text{ to } N_0) \tag{12b}$$

$$f^{0}(r) = \frac{1}{2}[f^{+}(r) + f^{-}(r)]^{0} \text{ (average)} \tag{12c}$$

Here, $f^{+}(r)$ is the reactivity index for a nucleophilic attack, $f^{-}(r)$ is the reactivity index for an electrophilic attack, and $f^{0}(r)$ is the reactivity index for a radical attack. Within the finite difference approximation, these relationships can be written as

$$f^{+}(r) = \rho_{N+1}(r) - \rho_N(r) \tag{13a}$$

$$f^{-}(r) = \rho_N(r) - \rho_{N-1}(r) \tag{13b}$$

$$f^{0}(r) = \frac{1}{2}[\rho_{N+1}(r) - \rho_{N-1}(r)] \tag{13c}$$

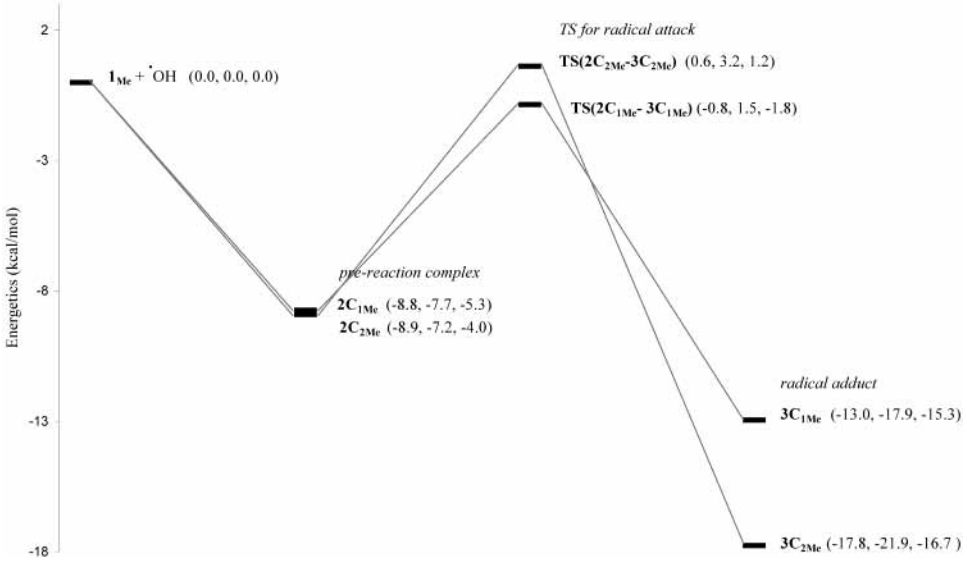

Figure 5. Potential energy profile for the hydroxyl radical addition mechanism in the C−N bond cleavage pathway of the CH_3-substituted azo dye at the B3LYP/6-31G(d) level. Relative energies in parentheses in the format of (B3LYP/6-31G(d), MPW1k/6-31+G(d,p)//B3LYP/6-31G(d), and IEFPCM). (0.0 kcal/mol on the relative energy axis corresponds to $\mathbf{1_{Me}}$ + •OH = (−1386.059447, −1385.81679, −1386.395475) hartrees.)

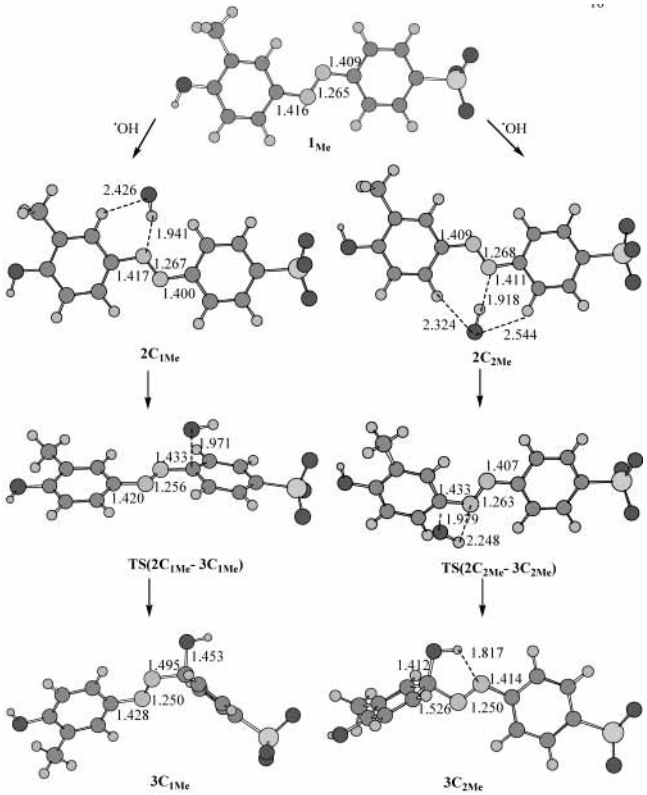

Figure 6. Optimized structures for hydroxyl radical addition in the C−N cleavage pathway of CH_3-substituted azo dye $\mathbf{1_{Me}}$.

A condensed form of these functions employs the atomic populations:[27]

$$f^{+} = q_k(N+1) - q_k(N) \tag{14a}$$

$$f^{-} = q_k(N) - q_k(N-1) \tag{14b}$$

$$f^{0} = \frac{1}{2}[q_k(N+1) - q_k(\mathrm{N}-1)] \tag{14c}$$

Methodology

Gaussian 98 has been employed for the calculation of geometries and energies.[28] Optimizations were performed at the B3LYP/6-31G(d) level of theory. According to the benchmark studies for radical addition reactions to double bonds, the B3LYP functional even with a 6-31G(d) basis set was found to give similar or better geometries and energies than MP2 calculations and similar results to QCISD with the same basis set.[29−31] It is also well known that in DFT calculations, the choice of the level of theory is more important than the choice of the basis set. Going to larger basis sets does not significantly affect the barrier heights and geometries. Therefore, for the azo dyes, which are relatively large in size, B3LYP/6-31G(d) is a good trade off between computer time and accuracy. Ground-state and transition-state structures have been confirmed by frequency analyses at the same level. Transition structures have been characterized by having one imaginary frequency that belonged to the reaction coordinate, corresponding to a first-order saddle point. IRC calculations have been performed for these transition geometries, and corresponding minima have been confirmed. Zero-point vibrational energies (ZPEs) were calculated at the B3LYP/6-31G(d) level; these were not scaled because they were used only for comparing possible reaction mechanisms. Reaction barrier heights were also determined by calculations at the MPW1K-6-31+G(d,p)//B3LYP/6-31G(d) level of theory. MPW1K[32] is a relatively new hybrid Hartree−Fock density functional method involving a single parameter that predicts significantly more accurate barrier heights. The MPW1K functional has been optimized against a database of barrier heights and reaction energies, and according to the available benchmark studies, it performs very well in predicting transition geometries and energies. However, it was parametrized with respect to a relatively large basis set and was suggested to be used with the same one for the best efficiency. This approach was not computationally affordable for the present purposes because of the size of the molecules. However, though MPW1K might perform better, the B3LYP functional also performs well and is widely used in predicting transition states[33,34]and hydrogen-bonded complexes.[35−39] In some cases, the transition-state geometries obtained by these two functionals resemble each other.[40] Therefore, the MPW1K-6-31+G(d,p)//B3LYP/6-31G-(d) methodology seems to be optimal for the present case.

Solvent effects were modeled using the integral equation formalism (IEF) polarized continuum model (PCM) of Tomasi

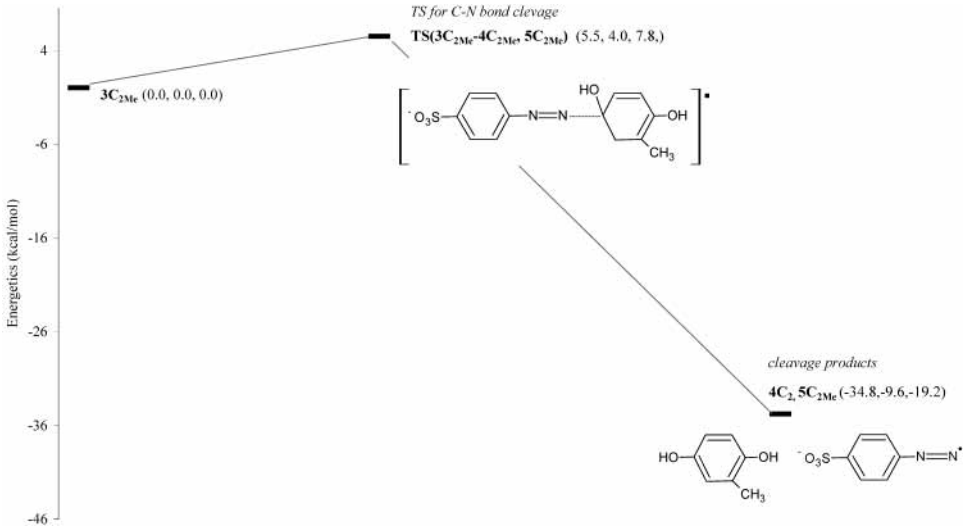

Figure 7. Potential energy profile for the C−N bond cleavage mechanism after the formation of a radical adduct for CH_3-substituted azo dye at B3LYP/6-31G(d) level. Relative energies in parentheses in the format of (B3LYP/6-31G(d), MPW1k/6-31+G(d,p)//B3LYP/6-31G(d), and IEFPCM) (0.0 kcal/mol on the relative energy axis corresponds to $\mathbf{3C_{2Me}}$ = (−1386.087742, −1386.0776593, −1386.413981) hartrees.

SCHEME 2: N−N Bond Cleavage Mechanism (X = Cl, Me)

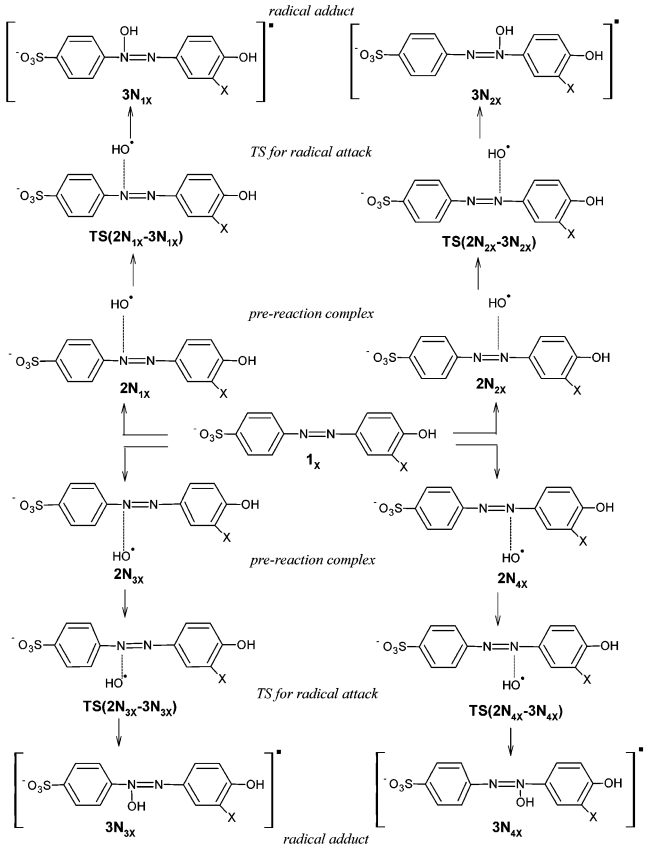

et al.[41] within self-consistent reaction field (SCRF) theory by means of single-point calculations based on the gas-phase geometries. Electronic populations for the calculation of Fukui indices were obtained from Mulliken population analysis[42] and natural population analysis.[43]

Results and Discussion

I. C−N Cleavage Mechanism for 2-Chloro and 2-Methyl Substituted Derivatives. Scheme 1 represents the proposed hydroxyl radical addition mechanism in C−N bond cleavage pathway for both derivatives in the form of a flowchart.

*A. 2-Chloro-4-(4′-sulfophenylazo)phenol (**1Cl**).* Hydroxyl Radical Addition. Figures 1 and 2 represent, respectively, the potential energy profile and the optimized structures for radical addition in the C−N bond cleavage mechanism of the 2-chloro-substituted azo dye (**1Cl**) in vacuum and in water. Because of the presence of substituents on the rings, the C atoms bearing the azo linkage are no longer equivalent, as in our previous study with the azobenzene molecule.[16] Therefore, there are now two possible sites that hydroxyl radicals might attack (or two subpathways that can end up with C−N bond cleavage): either the carbon atom of the ring with the sulfonyl group or the carbon atom of the ring with *m*-Cl and *p*-OH groups through transition states **TS(2C1Cl-3C1Cl)** (with −O···C− distance of 1.964 Å) and **TS(2C2Cl-3C2Cl)** (with −O···C− distance of 1.966 Å), respectively. There is a 1.2 kcal/mol energy difference between these two proposed transition states, the latter being more favorable probably because of the weak hydrogen-bond type of interaction (−N···H− distance: 2.254 Å) between the hydrogen of hydroxyl radical and an azo nitrogen that is not present in the former case. These transition states proceed to prereaction complexes formed by hydrogen bonding between the same radical hydrogen and azo nitrogen pair as well as by relatively weaker hydrogen bonds between the ring hydrogens and the oxygen of the radical.

In addition to this difference in barrier heights, the difference between the reaction energies for the initial attack is 9.0 kcal/mol, again, in favor of the latter subpathway because of the strong hydrogen bonding (**3C2Cl**) lowering the energy.

Cleavage of the C−N Bond. To gain a better insight into the C−N cleavage mechanism of the chloro-substituted azo dye, we further modeled the cleavage of the C−N bond, starting with the **3C2Cl** compound as a representative of the radical adducts formed (Figures 3 and 4). In the transition state **TS-(3C2Cl-4C2C,5C2Cl)**, the −C···N− distance increases to 1.819 Å, and the bond is broken, leading to the products *p*-sulfonylphenyldiazene (**4C2**) and *m*-chloro-*p*-hydroxylphenol (**5C2Cl**).

*B. 2-Methyl-4-(4′-sulfophenylazo)phenol (**1Me**).* Hydroxyl Radical Addition. In the same manner, Figures 5 and 6 represent, respectively, the potential energy profile and the optimized structures for the hydroxyl radical addition mechanism in the C−N bond cleavage pathway of the 2-methyl-substituted azo

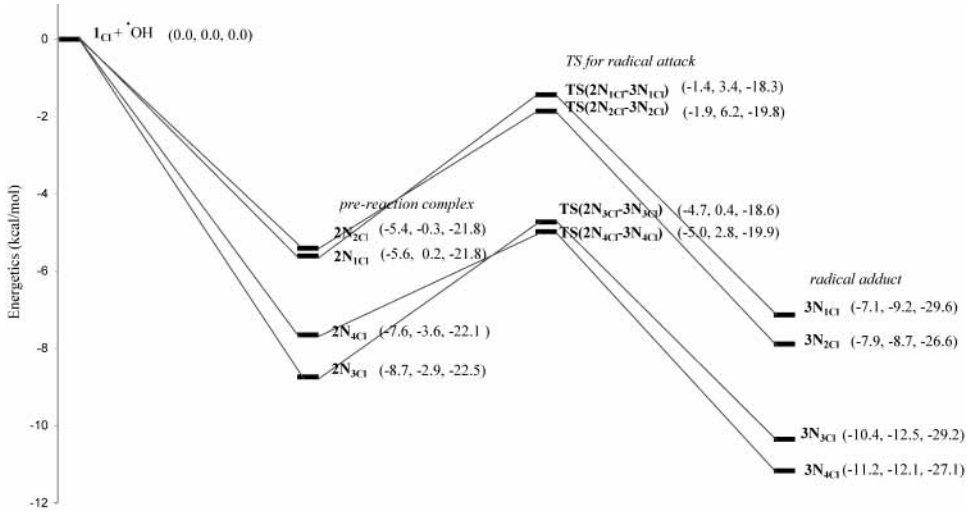

Figure 8. Potential energy profile for the hydroxyl radical addition mechanism in the N−N bond cleavage pathway of the Cl-substituted azo dye at the B3LYP/6-31G(d) level. Relative energies in parentheses in the format of (B3LYP/6-31G(d), MPW1k/6-31+G(d,p)//B3LYP/6-31G(d), and IEFPCM). (0.0 kcal/mol on the relative energy axis corresponds to $\mathbf{1_{Cl}}$ + •OH = (−1806.377834, −1806.138183, −1806.670002) hartrees.)

dye ($\mathbf{1_{Me}}$) in vacuum and in water. With the methyl group as the substituent, the energetic order of the transition states is reversed compared to the previous case, and the carbon atom of the ring with sulfonyl group becomes more susceptible to the attack of the hydroxyl radical by 1.5 kcal/mol.

The −C···O− distance is 1.979 Å for **TS($2C_{Me}$-$3C_{1Me}$)** and 1.979 Å for **TS($2C_{Me}$-$3C_{2Me}$)**, leading to relatively earlier transition states than the Cl-substituted case. This is in accord with the Hammond postulate,[44] which states that a more exothermic reaction will have an earlier transition state rather than a less exothermic reaction; the C−N cleavage mechanism for CH_3-substituted azo dye is more exothermic than the one for Cl-substituted azo dye.

Cleavage of the C−N Bond. The steps following the initial radical addition mechanism through the C−N bond cleavage have been modeled where the −C···N− distance increases to 1.824 Å through the transition state **TS($3C_{2Me}$-$4C_2$,$5C_{2Me}$)** and the bond is broken leading to products *p*-sulfonylphenyldiazene ($\mathbf{4C_2}$) and *m*-methyl-*p*-hydroxylphenol ($\mathbf{5C_{2Me}}$). (Figures 7 and 1S)

For both derivatives, $\mathbf{1_{Cl}}$ and $\mathbf{1_{Me}}$, further refinement of energies at the MPW1K/6-31+G(d,p)//B3LYP/6-31G(d) level has increased the barrier heights by 2.4−3.0 kcal/mol; however, the reaction energies for the formation of the adducts have become more exothermic by 3.8−4.9 kcal/mol.

II. N−N Cleavage Mechanism for 2-Chloro- and 2-Methyl-Substituted Derivatives. Scheme 2 represents the proposed hydroxyl radical addition mechanism in the N−N bond cleavage pathway for both derivatives in the form of a flowchart.

A. 2-Chloro-4-(4′-sulfophenylazo)phenol ($\mathbf{1_{Cl}}$). Hydroxyl Radical Addition. Figures 8 and 9 represent, respectively, the potential energy profiles and optimized structures of the adduct formation mechanism for the 2-chloro-substituted azo dye ($\mathbf{1_{Cl}}$) in vacuum and in water at the B3LYP/6-31G(d) level of theory. In the C-attack case, because the hydroxyl radical approaches the C atom in a perpendicular direction to the plane of the ring, there are two nonequivalent attack sites, one for each carbon, as •OH approaches from the upper or lower part of the molecular plane. However, because the hydroxyl radical approaches the N atom along the planar sp^2 lobes, there is a difference between the left and right directions due to the presence of a meta substituent. Thus, the hydroxyl radical can add to the N═N bond via four different transition structures by having two nonequivalent sites of attack for each of the two nonequivalent N atoms. The energies of pre-reaction complexes, transition states, and adducts have been found to be lower by ∼3 kcal/mol when the

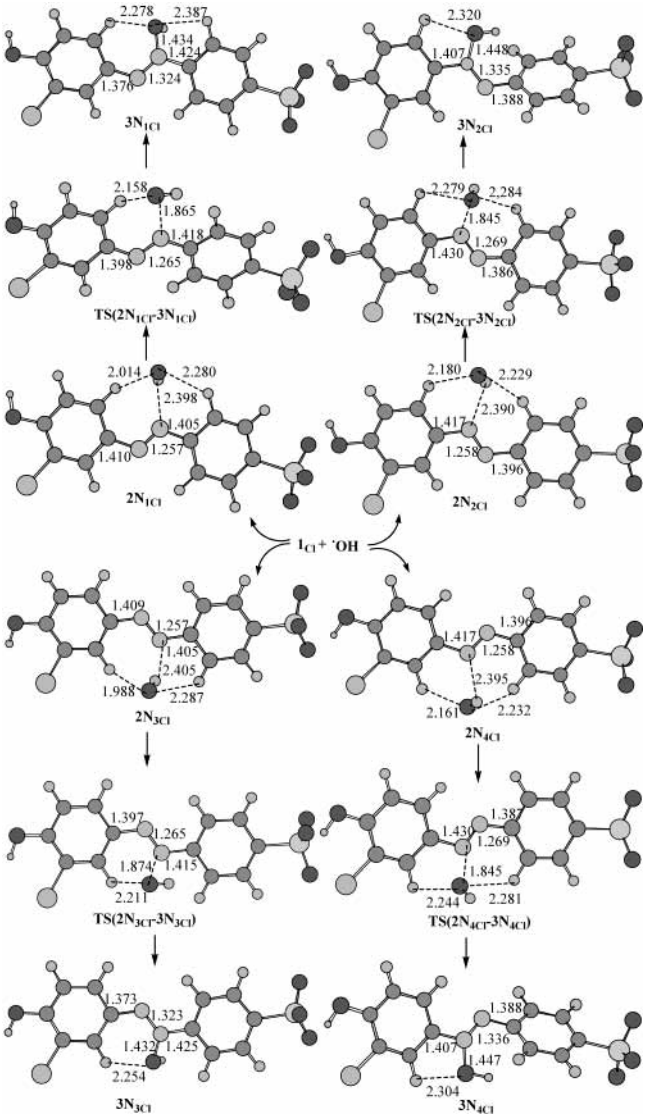

Figure 9. Optimized structures for hydroxyl radical addition in the N−N cleavage pathway for Cl-substituted azo dye $\mathbf{1_{Cl}}$.

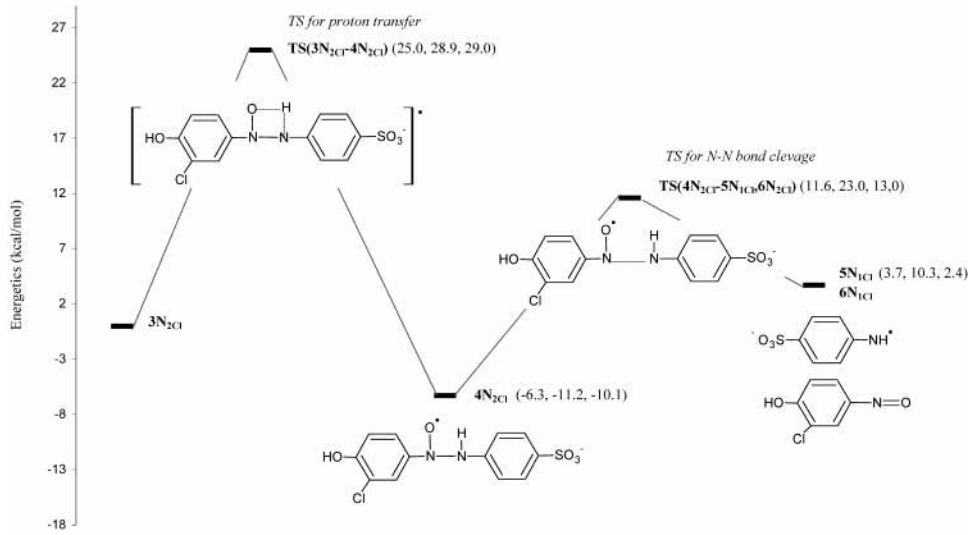

Figure 10. Potential energy profile for the N−N bond cleavage mechanism after the formation of radical adduct for the Cl-substituted azo dye at the B3LYP/6-31G(d) level. Relative energies in parentheses in the format of (B3LYP/6-31G(d), MPW1k/6-31+G(d,p)//B3LYP/6-31G(d), and IEFPCM). (0.0 kcal/mol on the relative energy axis corresponds to $\mathbf{3N_{2Cl}}$ = (−1806.389196, −1806.34853019, −1806.683594) hartrees.)

radical approaches the molecule from the side of the Cl substituent, $\mathbf{N_3}$ and $\mathbf{N_4}$, rather than from the opposite direction probably because of the stronger hydrogen bonds between the O atom of the hydroxyl radical and ring hydrogens.The −N···O− distance varies in the range of 2.381−2.398 Å in the prereaction complex to 1.845−1.874 Å in the transition states to reach the N−O single bond of 1.434−1.448 Å in the adducts.

Cleavage of the N−N bond. Figures 10 and 11 show the potential energy profile and the optimized structures, respectively, for the subsequent N−N cleavage mechanism after the formation of one of the N-attack adducts of Cl-substituted dye. This starting adduct was chosen arbitrarily. It includes a proton transfer from the hydroxyl group to the nitrogen atom as an intermediate step. Concerning the energetically high proton-transfer reaction in the N−N bond cleavage mechanism, a supermolecule approach has been proposed in our previous study[16] where a water molecule from the first solvation shell assists the proton transfer and lowers its energy through a subsequent cyclic rotational transition state due to the cooperative hydrogen bonding.

*B. 2-Methyl-4-(4′-sulfophenylazo)phenol (**1**$_{Me}$).* Hydroxyl Radical Addition. In the case of the potential energy surface for the 2-methyl-substituted derivative ($\mathbf{1_{Me}}$), unlike the Cl-substitution, there is no particular preference for one subpathway over the other. As can be seen in Figure 12, the prereaction complexes, transition states, and initial-attack products differ in energy at most by 0.4, 0.5, and 0.7 kcal/mol, respectively. The −N···O− distance varies in the range of 2.371−2.403 Å for the complexes, to 1.839−1.865 Å in the transition states, and to 1.435−1.448 Å in the adducts. Figure 13 shows the optimized structures for the radical addition mechanism.

Cleavage of the N−N bond. Figures 14 and 2S, respectively, show the potential energy profile and the optimized structures for the subsequent N−N cleavage mechanism after the formation of one of the N-attack adducts of the CH_3-substituted dye.

In a similar way, with the case of C−N cleavage, employment of the MPW1K/6-31+G(d,p)//B3LYP/6-31G(d) calculations have increased the barrier heights by ∼4.8−8.1 kcal/mol for both Cl- and CH_3-substituted derivatives. The adduct formation mechanisms are more exothermic by 0.9−2.1 kcal/mol at this level.

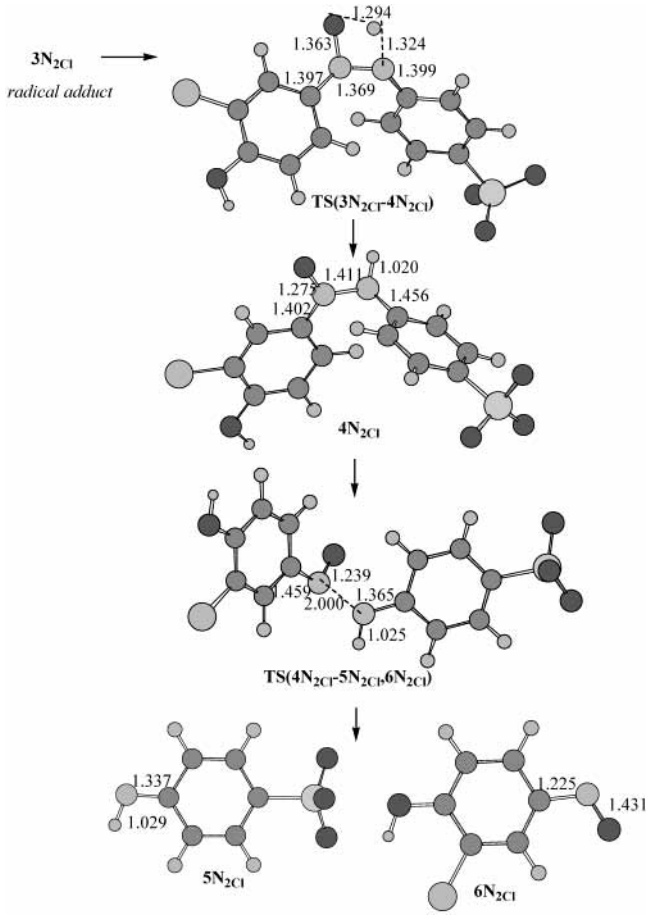

Figure 11. Optimized structures for the N−N cleavage pathway after the formation of a radical adduct for Cl-substituted azo dye $\mathbf{1_{Cl}}$.

Comparison of Potential Energy Profiles: C versus N and Cl versus Methyl

Reactions of azo dyes with hydroxyl radicals are characterized by their relatively fast color disappearance and slow total mineralization rates.[45] In light of this experimental evidence, the oxidative degradation of the azo benzene molecule was modeled in our previous study,[16] and the comparison of the potential energy surfaces and the application of local reactivity

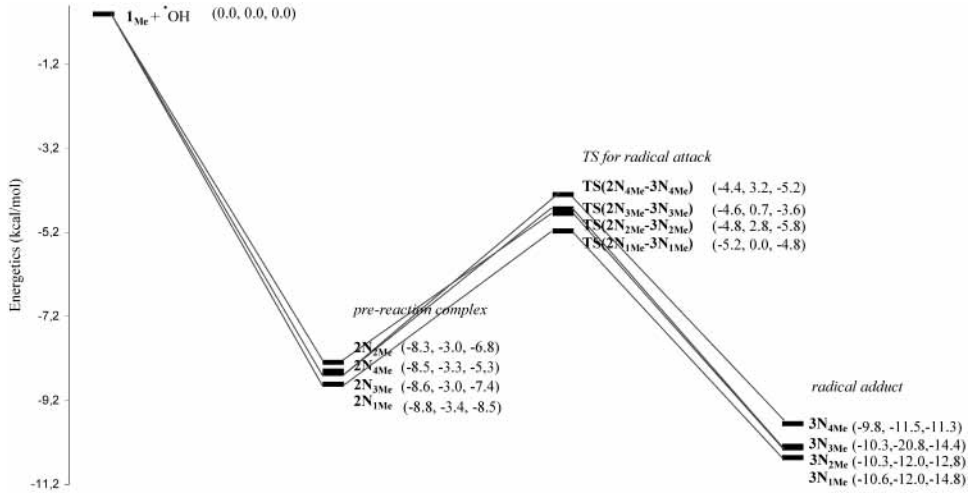

Figure 12. Potential energy profile for the hydroxyl radical addition mechanism in the N−N bond cleavage pathway of the CH_3-substituted azo dye at the B3LYP/6-31G(d) level. Relative energies in parentheses in the format of (B3LYP/6-31G(d), MPW1k/6-31+G(d,p)//B3LYP/6-31G(d), and IEFPCM). (0.0 kcal/mol on the relative energy axis corresponds to $\mathbf{1_{Me}}$ + •OH = (−1386.059447, −1385.81679, −1386.395475) hartrees.)

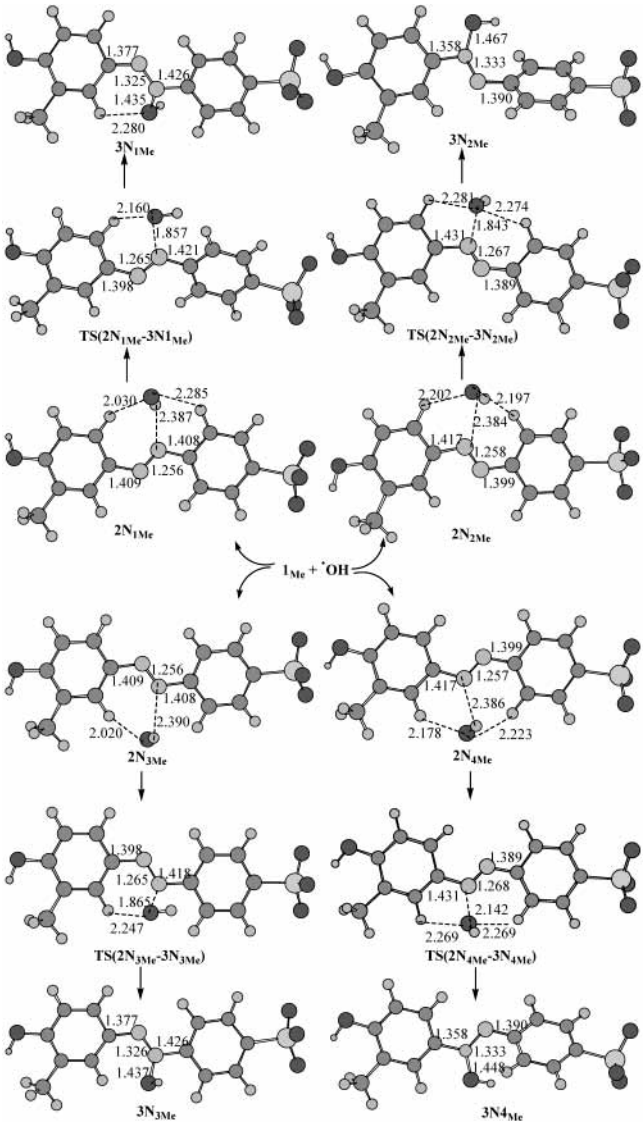

Figure 13. Optimized structures for hydroxyl radical addition in the N−N cleavage pathway of CH_3-substituted azo dye $\mathbf{1_{Me}}$.

indices pointed to a reaction mechanism in which the N−N bond was broken in preference to the C−N bond. The same trend has been observed for the proposed reaction pathways in the case of 2-chloro- and 2-methyl-substituted derivatives of azo benzene in this study.

For the Cl-substituted derivative, the highest-energy transition state of the initial radical attack for the N−N cleavage mechanism (**TS(2N$_{1Cl}$-3N$_{1Cl}$)**) is still 2.7 kcal/mol lower in energy than the lowest-energy transition state of the C−N cleavage mechanism (**TS(2C$_{2Cl}$-3C$_{2Cl}$)**) at the B3LYP/6-31G-(d) level of theory. However, when the barrier heights (E_a) of the following bond cleavage steps are compared, this situation is reversed (E_a for **TS(3N$_{2Cl}$-4N$_{2Cl}$)** − E_a for **TS(3C$_{2Cl}$-4C$_{2Cl}$)** = 24.5 kcal/mol), pointing to a slow mineralization for the N−N cleavage mechanism. For the CH_3-substituted derivative, there is a larger energy difference between the highest- and lowest-energy initial attack transition states of two pathways (ΔE [**TS-(2C$_{1Me}$-3C$_{1Me}$)** − **TS(2N$_{4Me}$-3N$_{4Me}$)**] = 3.4 kcal/mol) in favor of the N−N cleavage mechanism. As in the case of Cl substitution, the energy difference between the barrier energies of the steps that follow points out a slow mineralization for the N−N cleavage mechanism (E_a for **TS(2N$_{1Me}$-3N$_{1Me}$)** = 25.6 kcal/mol) and a fast reaction for C−N bond cleavage (E_a for **TS(3C$_{2Me}$-4C$_{2Me}$)** = 2.1 kcal/mol).

Therefore, in both of these cases, the N−N cleavage mechanism, with a smaller barrier for the initial attack of the hydroxyl radicals that mimics the experimentally observed fast disappearance of color and with a larger activation barrier for the following bond cleavage that mimics the experimentally observed slow mineralization rate, appears to be the preferred pathway over the C−N cleavage mechanism.

The presence of a dielectric medium has a stabilizing effect, decreasing the overall energy for both C−N and N−N bond cleavage mechanisms, but still the transition states for the former lie higher in energy than those for the latter, and the same trend has been observed in the following steps of the cleavage.

Experimentally, the degradation yield for the Cl-substituted derivative was observed to be higher than the CH_3-substituted one.[3] However, the comparison of the N−N cleavage mechanism potential energy surfaces in vacuum and in water for Cl- and CH_3-substituted derivatives has given different reactivity trends. In vacuum, similar potential energy surfaces have been obtained for both derivatives, with the methyl-substituted derivative being more reactive. This is contradictory to the experimental results. However, in the presence of a solvent, the reactivity trend is reversed in favor of the Cl-substituted dye. A dielectric medium stabilizes the transition states for the N−N

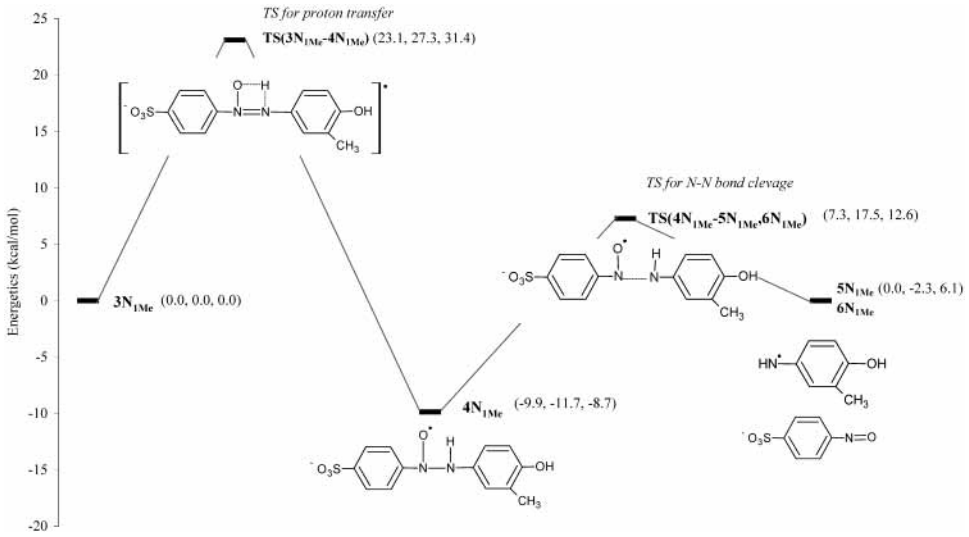

Figure 14. Potential energy profile for the N−N bond cleavage mechanism after the formation of the radical adduct for the CH_3-substituted azo dye at the B3LYP/6-31G(d) level. Relative energies in parentheses in the format of (B3LYP/6-31G(d), MPW1k/6-31+G(d,p)//B3LYP/6-31G(d), and IEFPCM). (0.0 kcal/mol on the relative energy axis corresponds to $\mathbf{3N_{2Me}}$ = (−1386.076276, −1386.409992, −1386.0617805) hartrees.)

TABLE 1: Chemical Reactivity Indices for Cl- and CH_3-Substituted Derivatives ($\mathbf{1_{Cl}}$ and $\mathbf{1_{Me}}$) and for the OH Radical at the B3LYP/6-31(d) Level

	$\mathbf{1_{Cl}}$ (S = 12.4013)				$\mathbf{1_{Me}}$ (S = 13.2342)			
	$f^0_{Mulliken}$	f^0_{NPA}	$s^0_{Mulliken}$	s^0_{NPA}	$f^0_{Mulliken}$	f^0_{NPA}	$s^0_{Mulliken}$	s^0_{NPA}
1 C	0.0004	0.0040	0.0055	0.0495	0.0046	0.0042	0.0612	0.0553
2 N	0.0516	0.0544	0.6399	0.6751	0.0551	0.0549	0.7296	0.7260
3 N	0.0510	0.0569	0.6325	0.7056	0.0577	0.0576	0.7642	0.7619
4 C	−0.0018	0.0004	−0.0225	0.0051	0.0015	0.0015	0.0200	0.0194
5 C	0.0138	0.0181	0.1706	0.2248	0.0312	0.0313	0.4136	0.4148
6 C	0.0337	0.0352	0.4176	0.4364	0.0377	0.0374	0.4991	0.4953
7 H	0.0477	0.0493	0.5911	0.6115	0.0495	0.0494	0.6556	0.6544
8 H	0.0192	0.0120	0.2387	0.2476	0.0212	0.0213	0.2807	0.2824
9 H					0.0155	0.0156	0.2047	0.2066
10 H					0.0273	0.0274	0.3614	0.3623
11 H					0.0273	0.0274	0.3619	0.3628
	OH radical (S = 3.3904)							
O	0.7736	0.7736	2.6228	2.6228				

cleavage mechanisms of the Cl-substituted dye more than those of the CH_3-substituted one. Also, when the full paths are compared, the Cl-substituted dye was found to be more reactive for hydroxyl radical addition reactions in accordance with the experiment.

Another possible explanation for the experimental reactivity difference can be attributed to the presence of a competing reaction that would consume the hydroxyl radicals in the case of CH_3 substitutions but not in the case of Cl substitutions. Therefore, the competitive pathways have been determined by using chemical reactivity indices, and the relative energies of the corresponding transition states were compared with C−N and N−N bond cleavage mechanisms.

Competitive Pathways

Chemical Reactivity Indices. In the search for a competing reaction, chemical reactivity indices (Table 1) have been employed to have information about the most susceptible sites for hydroxyl radical attack. Figure 15 shows the numbering system that is used throughout the calculations. Sites with relatively low values are not shown in Table 1.

The hydroxyl radical can undergo mainly three types of addition reactions with azo dyes

(i) addition to the chromophore (1 C, 2 N, 3 N, and 4 C)

(ii) addition to the ring (5 C, 6 C)

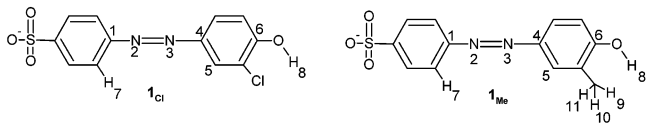

Figure 15. Numbering system used in modeling the competing pathways.

TABLE 2: Chemical Reactivity Indices for Cl- and CH_3-Substituted Derivatives and for the OH Radical at MPW1K/6-31 + G(d,p)//B3LYP/6-31(d) Level

	$\mathbf{1_{Cl}}$ (S = 12.4013)		$\mathbf{1_{Me}}$ (S = 13.2342)	
	$f^0_{Mulliken}$	$s^0_{Mulliken}$	$f^0_{Mulliken}$	$s^0_{Mulliken}$
1 C	0.0093	0.0958	0.0205	0.2175
2 N	0.0923	0.9482	0.0806	0.8563
3 N	0.0851	0.8750	0.0960	1.0199
4 C	−0.046	−0.4756	−0.0317	−0.3370
5 C	0.0119	0.1226	0.0564	0.5990
6 C	0.0598	0.6141	0.0288	0.3065
7 H	0.0364	0.3737	0.0358	0.3807
8 H	0.0141	0.1448	0.0161	0.1709
9 H			0.0087	0.0927
10 H			0.0220	0.2340
11 H			0.0220	0.2343
	OH radical (S=3.3904)			
O	0.7736	2.6228		

(iii) hydrogen abstraction (7 H, 8H, 9 H, 10 H, 11 H).

One-electron oxidation is also observed, especially when radiolysis is used as the advanced oxidation method.

In Tables 1 and 2, the specific sites have been selected on the basis of their softness values being close to that of the OH radical, on the basis of the local hard−soft acid−base (HSAB) principle formulated by Gazquez and Mendez,[46] which states that the interaction between two chemical species will not necessarily occur through their softest atoms but through those whose softnesses are approximately equal. When the same principle is employed, condensed fukui functions (f^0), being local reactivity descriptors, confirm the findings derived from the potential energy surface analysis in the sense that hydroxyl radicals prefer to attack the N atom rather than the C atom in the chromophore. A comparison of the local softness values[47] (s^0) for Cl- and CH_3-substituted derivatives predicts a reactivity difference between the ring addition reactions of these two compounds through site C5, the latter being more reactive.

TABLE 3: Energy-Scales for the Transition States of the Competing Reactions for the Cl-Substituted Dye

TS	B3LYP	MPW1K// B3LYP	IEFPCM// B3LYP	
TS($2C_{1Cl}-3C_{1Cl}$)	7.5	7.1	6.6	attack on C bearing azo link
TS($2C_{2Cl}-3C_{2Cl}$)	6.3	6.4	7.5	
TS(H 7-attack)$_{Cl}$	3.7	8.5	10.4	ring-hydrogen abstraction
TS($2N_{1Cl}-3N_{1Cl}$)	3.6	5.5	1.6	attack on N of azo link
TS($2N_{2Cl}-3N_{2Cl}$)	3.1	8.3	0.1	
TS(C 5-attack)$_{Cl}$	0.4	**0.0**	2.3	addition to the ring
TS($2N_{3Cl}-3N_{3Cl}$)	0.3	2.5	1.3	attack on N of azo link
TS($2N_{4Cl}-3N_{4Cl}$)	**0.0**	4.9	**0.0**	

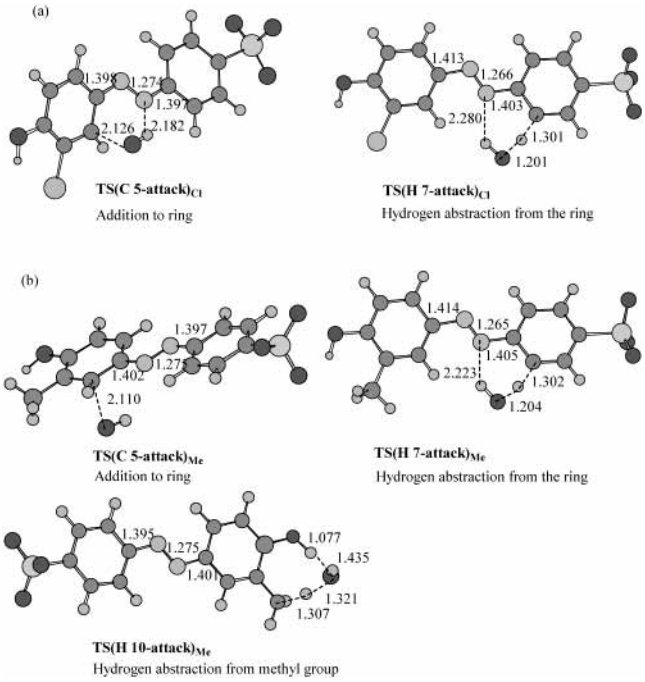

Figure 16. Optimized structures for the transition states of the completing reactions for (a) Cl- (b) CH_3-substituted derivatives.

However, the reaction of C5 for the Cl-substituted derivative was found to be more favorable—even more favorable than some N attack reactions (Table 3). It may be that the transition state for this derivative (**TS(C 5-attack)$_{Cl}$**) is stabilized by hydrogen bonding between the hydrogen of the hydroxyl radical and the nitrogen of the azo group, whereas no hydrogen bonding was observed for the CH_3 derivative case (**TS(C 5-attack)$_{Me}$**) (Figure 16). This draws attention to the point that although chemical reactivity descriptors are useful tools in predicting the course of a reaction, in some cases special interactions such as hydrogen bonding may interfere with the predictions. It must also be noted that, having exothermic reactions for the initial attack (both ΔE_{rxn} **(C 5-attack)$_{Cl}$** and ΔE_{rxn} **(C 5-attack)$_{Me}$** are −28.3 kcal/mol), addition to the ring reactions seriously compete with addition to the chromophore reactions for both derivatives in a vacuum. The exothermicity may be due to the stabilization of the initial attack products via hydrogen bonding (Figure 3S). In solution, however, addition to the ring is a concern only for Cl substitution (ΔE [**TS(C 5-attack)$_{Cl}$ − 1$_{Cl}$**] = −17.6 kcal/mol) but not for CH_3 (ΔE [**TS(C 5-attack)$_{Me}$ − 1$_{Me}$**] = +15.0 kcal/mol) substitution (Tables 3 and 4).

TABLE 4: Energy-Scales for the Transition States of the Competing Reactions for CH_3-Substituted Dye

TS	B3LYP	MPW1K// B3LYP	IEFPCM// B3LYP	
TS($2C_{2Cl}-3C_{2Cl}$)	17.2	7.2	16.5	attack on C bearing azo link
TS($2C_{1Cl}-3C_{1Cl}$)	15.8	5.5	13.5	
TS(H 7-attack)$_{Me}$	14.9	9.7	17.9	ring-hydrogen abstraction
TS(C 5-attack)$_{Me}$	12.5	3.1	30.3	addition to the ring
TS($2N_{4Me}-3N_{4Me}$)	12.2	7.2	10.1	attack on N of azo link
TS($2N_{3Me}-3N_{3Me}$)	12.0	4.7	11.7	
TS($2N_{2Me}-3N_{2Me}$)	11.8	6.8	9.5	
TS($2N_{1Me}-3N_{1Me}$)	11.4	4.0	10.5	
TS(H 10-attack)$_{Me}$	**0.0**	**0.0**	**0.0**	hydrogen abstraction from CH_3 group

C6 is another site where addition to the ring may take place, and the local softness value for this atom points to the CH_3-substituted derivative to be more reactive for an attack through this site. However, one of the products of such a substitution reaction is another hydroxyl radical, and the total number of hydroxyl radicals in the environment does not change. Therefore, this is probably not the competing reaction that lowers the yield in dye degradation for methyl substitution. Another competing reaction is the abstraction of ring hydrogen H 7. A comparison of the local softness values indicates the CH_3-substituted derivative to be relatively more reactive toward this type of reaction (Table 1). Actually, the transition state **TS(H7-attack)$_{Me}$** was found to be located lower in energy than the transition state **TS(H7-attack)$_{Cl}$** by 0.45 and 0.7 kcal/mol in vacuum at the B3LYP/6-31G(d) and MPW1K/6-31+G(d,p) levels of theory, respectively, with respect to the coresponding reactants. These differences are not enough to explain the huge difference in the experimental yields. Besides, in a dielectric medium, this trend is reversed. Therefore, this probably is not the competing reaction being searched for either.

Indeed, the key mechanism of competition appeared to be another hydrogen abstraction reaction: hydrogen abstraction from the methyl group itself. The hydrogen atoms of the CH_3 group are good candidates to consume hydroxyl radicals. Even though they seem to be less reactive than ring hydrogens on the basis of their local softness values (Table 1), their transition state for the abstraction mechanism was found to be energetically more favorable because of a hydrogen-bonding network (Figure 16) in a seven-membered ring. For example, in vacuum, **TS(H 10-attack)$_{Me}$** is 11.5 kcal/mol lower in energy than **TS($2N_{1Me}$-$3N_{1Me}$)**, being the closest neighbor transition state over the potential energy surface. The same trend has been observed in a solvent, with an energy difference of 2 kcal/mol. Also, it is a highly exothermic reaction in terms of the initial attack with a reaction energy of −29.4 kcal/mol, probably because of the hydrogen bonding present in the product (Figure 3S). Therefore, it can be concluded that the CH_3-substituted derivative has a lower yield for the dye degradation reaction, that is, for addition to the chromophore reaction, than the Cl-substituted derivative also because of the presence of a competing hydrogen abstraction mechanism that consumes the hydroxyl radicals in the environment.

Conclusions

The purpose of this study was to determine the most plausible mechanism for the hydroxyl radical addition to substituted azo dyes as well as to explain the pronounced difference in reaction

yields for Cl- and CH_3-substituted derivatives. Comparing the potential energy surfaces and employing the local reactivity descriptors have shed light onto both of these issues: as in the case of the azo benzene molecule, the N−N bond cleavage mechanism has been found to be the more preferable pathway over the mechanism where a C−N bond is broken for both derivatives. The greater reactivity of the Cl-substituted derivative has also been explained by the presence of a competing reaction for the CH_3-substituted derivative, consuming the hydroxyl radicals in the environment. It has also been seen that local reactivity indices are useful tools for predicting the susceptible sites for a reaction to proceed but, as expected, cannot describe the secondary interactions such as hydrogen bonding.

Acknowledgment. We thank Boğaziçi Üniversitesi Bilimsel Araştırma Projeleri (BAP 02B501) and Devlet Planlama Teşkilatı (DPT 98K 120900) for financial support. A.S.Ö acknowledges Boğaziçi Üniversitesi Vakfı Akademik Faaliyetler Destek Fonu for supporting her visit to the Free University of Brussels (VUB). A.S.Ö and V.A. acknowledge the ASMA (Advanced System for Multi-computer Applications) Project at Bogazici University and also project no. 03R104 "Biyolojik Sistemler ve Polimerik Malzemelerin Modelenmesine Yönelik Üniversite Ölçekli Bilimsel Hesaplama Şebekesi Geliştirilmesi". F.D.P. and P.G. acknowledge the Fund for Scientific Research-Flanders (Belgium) (FWO) and the Free University of Brussels (VUB) for continuous support.

Supporting Information Available: Optimized structures for C−N and N−N cleavage pathways for $\mathbf{1_{Me}}$ (CH_3-substituted azo dye) and optimized structures for the products of the competing reactions. This material is available free of charge via the Internet at http://pubs.acs.org.

References and Notes

(1) Spadaro, J. T.; Isabelle, L.; Renganathan, V. *Environ. Sci. Technol.* **1994**, *28*, 1389−1393.
(2) Vinodgopal, K.; Kamat, P. V. In *Environmental Applications of Ionizing Radiation*; Cooper, W. J., Curry, R. D., O'Shea, K. E., Eds.; John Wiley & Sons: New York, 1998; pp 587−599.
(3) Nam, S.; Renganathan, V.; Tratnyek, P. G. *Chemosphere* **2001**, *45*, 59−65.
(4) Bandara, J.; Nadtochenko, V.; Kiwi, J.; Pulgarin, C. *Water Sci. Technol.* **1997**, *35*, 87−93.
(5) Galindo, C.; Jacques, P.; Kalt, A. *J. Photochem. Photobiol., A* **2000**, *130*, 35−47.
(6) Poulios, I.; Aetopoulou, I. *Environ. Technol.* **1999**, *20*, 479−487.
(7) Hustert, K.; Zepp, R. G. *Chemosphere* **1992**, *24*, 335−342.
(8) Tanaka, K.; Padermpole, K.; Hisanaga, T. *Water Res.* **2000**, *34*, 327−333.
(9) Nasr, C.; Vinodgopal, K.; Fisher, L.; Hotchandani, S.; Chattopadhyay, A. K.; Kamat, P. V. *J. Phys. Chem.* **1996**, *100*, 8436−8442.
(10) Das, S.; Kamat, P. V.; Padmaja, S.; Au, V.; Madison S. A. *J. Chem. Soc., Perkin Trans. 2* **1999**, 1219−223.
(11) Devi, L. G.; Krishnaiah, G. M. *J. Photochem. Photobiol., A* **1999**, *121*, 141−145.
(12) Destaillats, H.; Turjanski, A. G.; Estrin, D. A.; Hoffmann, M. R. *J. Phys. Org. Chem.* **2002**, *15*, 287−292.
(13) Panajkar, M. S.; Mohan, H. *Indian J. Chem., Sect. A* **1993**, *32*, 25−27.
(14) Joseph, J. M.; Destaillats, H.; Hung, H.; Hoffmann, M. R. *J. Phys. Chem. A* **2000**, *104*, 301−307.
(15) Tang, W. Z.; Zhang, Z.; An, H.; Quintana, M. O.; Torres, D. F. *Environ. Technol.* **1997**, *18*, 1−12.
(16) Ozen, A. S.; Aviyente, V.; Klein, R. A. *J. Phys. Chem. A* **2003**, *107*, 4898−4907.
(17) Parr, R. G.; Yang, W. *Density-Functional Theory of Atoms and Molecules*; Oxford University Press: New York, 1989.
(18) Koch, W.; Holthausen, M. C. *A Chemist's Guide to Density Functional Theory*; Wiley-VCH: Weinheim, Germany, 2001.
(19) Jensen, F. *Introduction to Computational Chemistry*; John Wiley & Sons: Chichester, U.K., 1999.
(20) (a) De Proft F.; Geerlings, P. *Chem. Rev.* **2001**, *101*, 1451−1464. (b) Geerlings, P.; De Proft, F.; Langenaeker, W. *Chem. Rev.* **2003**, *103*, 1793−1874.
(21) Chermette, H. *J. Comput. Chem.* **1999**, *20*, 129−154.
(22) Lim, M. H.; Worthington, S. E.; Dulles, F. J.; Cramer, C. J. Density Functional Calculations of Radicals and Diradicals. In *Density-Functional Methods in Chemistry*; Laird, B. B., Ross, R. B., Ziegler, T., Eds.; ACS Symposium Series, American Chemical Society: Washington, DC, 1996; Vol. 629, p 402.
(23) Bally, T.; Borden, W. T. Calculations on Open-Shell Molecules: A Beginner's Guide. In *Reviews in Computational Chemistry*; Lipkowitz, K. B., Boyd, D. B., Eds.; Wiley-VCH:New York, 1999; Vol. 13, p 1.
(24) Pearson, R. G. *J. Chem. Educ.* **1999**, *76*, 267−275.
(25) Pearson, R. G. *J. Chem. Educ.* **1987**, *64*, 561.
(26) Parr, R. G.; Yang, W. *J. Am. Chem. Soc.* **1984**, *106*, 4049−4050.
(27) Yang, W.; Mortier, W. J. *J. Am. Chem. Soc.* **1986**, *108*, 5708−5711.
(28) Frisch, M. J.; Trucks, G. W.; Schlegel, H. B.; Scuseria, G. E.; Robb, M. A.; Cheeseman, J. R.; Zakrzewski, V. G.; Montgomery, J. A., Jr.; Stratmann, R. E.; Burant, J. C.; Dapprich, S.; Millam, J. M.; Daniels, A. D.; Kudin, K. N.; Strain, M. C.; Farkas, O.; Tomasi, J.; Barone, V.; Cossi, M.; Cammi, R.; Mennucci, B.; Pomelli, C.; Adamo, C.; Clifford, S.; Ochterski, J.; Petersson, G. A.; Ayala, P. Y.; Cui, Q.; Morokuma, K.; Malick, D. K.; Rabuck, A. D.; Raghavachari, K.; Foresman, J. B.; Cioslowski, J.; Ortiz, J. V.; Stefanov, B. B.; Liu, G.; Liashenko, A.; Piskorz, P.; Komaromi, I.; Gomperts, R.; Martin, R. L.; Fox, D. J.; Keith, T.; Al-Laham, M. A.; Peng, C. Y.; Nanayakkara, A.; Gonzalez, C.; Challacombe, M.; Gill, P. M. W.; Johnson, B. G.; Chen, W.; Wong, M. W.; Andres, J. L.; Head-Gordon, M.; Replogle, E. S.; Pople, J. A. *Gaussian 98*, revision A.7; Gaussian, Inc.: Pittsburgh, PA, 1998.
(29) Wong, M. W.; Radom, L. *J. Phys. Chem. A* **1998**, *102*, 2237−2245.
(30) Fischer, H.; Radom L. *Angew. Chem., Int. Ed.* **2001**, *40*, 1340−1371.
(31) Suh, I.; Zhang, D.; Zhang, R.; Molina, L. T.; Molina, M. J. *Chem. Phys. Lett.* **2002**, *364*, 454−462.
(32) Lynch, B. J.; Fast, P. L.; Truhlar, D. G. *J. Phys. Chem. A* **2000**, *104*, 4811−4815.
(33) Durant, J. L. *Chem. Phys. Lett.* **1996**, *256*, 595−602.
(34) Bach, R. D.; Glukhovtsev, M. N.; Gonzalez, C.; Marquez, M.; Estévez, C. M.; Baboul, A. G.; Schlegel, H. B. *J. Phys. Chem. A* **1997**, *101*, 6092−6100.
(35) Tuma, C.; Boese, A. D.; Handy, N. C. *Phys. Chem. Chem. Phys.* **1999**, *1*, 3939−3947 (and supplementary information).
(36) Lozynski, M.; Rusinska-Roszak, D.; Mack, H. G. *J. Phys. Chem. A* **1998**, *102*, 2899−2903.
(37) Chandra, A. K.; Nguyen, M. T. *Chem. Phys.* **1998**, *232*, 299−306.
(38) Lundell, J.; Latajka, Z. *J. Phys. Chem. A* **1997**, *101*, 5004−5009.
(39) Cheng, J.; Kang, C.; Zhu, W.; Luo, X.; Puah, C. M.; Chen, K.; Shen, J.; Jiang H. *J. Org. Chem.* **2003**, *68*, 7490−7495.
(40) Zhao, J.; Zhang, R.; North, S. W. *Chem. Phys. Lett.* **2003**, 204−213.
(41) Tomasi, J.; Mennucci, B.; Cancés, E. *J. Mol. Struct.: THEOCHEM* **1999**, *464*, 211−226.
(42) Mulliken, R. S. *J. Chem. Phys.* **1955**, *23*, 1833; 1841; 2338; 2343.
(43) Reed, A. E.; Weinstock, R. B.; Weinhold, F. *J. Chem. Phys.* **1985**, *83*, 735−746.
(44) Pross, A. *Theoretical and Physical Principles of Organic Reactivity*; John Wiley & Sons: New York, 1995.
(45) Tezcanli-Guyer, G.; Ince, N. H. *Ultrason. Sonochem.* **2003**, *10*, 235−240.
(46) Gazquez, J. L.; Méndez, F. *J. Phys. Chem.* **1994**, *98*, 459.
(47) (a) Yang, W.; Parr, R. G. *Proc. Natl. Acad. Sci. U.S.A.* **1985**, *82*, 6723. (b) Lee, C.; Yang, W.; Parr, R. G. *J. Mol. Struct.: THEOCHEM* **1988**, *163*, 305.